

NE 533: Final Project

Aidan Furlong

April 28th, 2023

Work was performed to calculate the temperature profile for a 2-D RZ section of a Light Water Reactor (LWR) fuel pin with constant thermal properties and a coolant temperature varied axially over the 100 cm span with the provided equation and constant $T_{in} = 500\text{K}$. Problem dimensions and geometry were provided with fuel, gap, and clad thicknesses of 0.5, 0.002, and 0.1 centimeters respectively. Mass flowrate, LHR_0 , h_{cool} , and specific heat were held at $2.5 \times 10^{-1} \frac{\text{kg}}{\text{s}}$, $3.50 \times 10^2 \frac{\text{W}}{\text{cm}^2\text{K}}$, $2.65 \frac{\text{W}}{\text{cm}^2\text{K}}$, and $4.200 \times 10^3 \frac{\text{J}}{\text{kg}\text{K}}$. These values are typical for a ceramic uranium dioxide-fueled LWR system.

A total of six simulations were run with varying conditions for two main solutions: steady state and transient. In both of these, there were runs with a uniform LHR and axially-variant LHR. In addition, the steady state cases had branches for constant thermal conductivity and temperature-dependent thermal conductivity of the fuel. In parts one and two of this project, work was focused on getting temperature profiles over the fuel pin radius and in transient conditions. This document will discuss the coupling of this thermal-related work to tensor mechanics to account for thermal expansion and associated stresses.

Constant thermal conductivities for fuel, gap, and clad materials were approximated and held constant at 0.03, 0.0026, and $0.17 \frac{\text{W}}{\text{cm}\text{K}}$ respectively. In temperature-dependent thermal conductivity cases, the thermal conductivity of the helium gap was held constant with the fuel and clad material k_{th} values updated with PiecewiseLinear functions. Thermal conductivity data for the uranium dioxide were taken from Nishijima et. al. [1] and Zircaloy from Cleveland et. al. [2] over the expected temperature ranges with an average step size of 100 K. Between these values, the properties are interpolated linearly.

Implementing the Tensor Mechanics module into the previously-built heat conduction system, thermal expansion and isotropic elasticity were considered for each of the material regions. The von mises stress was then calculated in the fuel and clad regions. The gap region was omitted from this calculation as it is can be approximated as an unconstrained fluid with a plenum reservoir at the top of the pin system. The thermal boundary conditions were maintained as those identified in Part II of the project, with a zero-flux Neumann boundary on the left centerline and outer cladding temperature

Dirichlet boundary on the right (axially dependent on the coolant heat transfer previously described). Mechanically, the system had displacement pinned at the lower left-hand side of the system to allow for thermal expansion vertically and radially as a real-life system would experience with a hold-down spring in the above plenum. The lower boundary had vertical displacement set to zero as well. To implement this methodology, an additional set of parameters were required to describe the mechanical properties of each material, listed in Table 1 below.

Table 1: Mechanical parameters and values for each material

Parameter	UO_2	He_2	Zircaloy
Bulk Modulus	-	27 MPa	-
Coeff., Thermal Expansion	$8 \times 10^{-6} \text{ K}^{-1}$	$3.7 \times 10^{-3} \text{ K}^{-1}$	$6 \times 10^{-6} \text{ K}^{-1}$
Poisson's Ratio	0.25	-	0.37
Reference Temperature	300 K	300 K	300 K
Young's Modulus	290 GPa	-	99.3 GPa

In terms of numerically solving these problems, there were 301 horizontal elements and 20 vertical elements in each mesh. Larger values were considered to enhance the resolution of this model, but due to convergence issues were reduced to these values. A Single Matrix Preconditioner (SMP) was then implemented in conjunction with MOOSE's automatic scaling methodology to further enhance convergence rates and reduce instances of non-linear divergence errors. The default tolerance for both linear and non-linear residuals were also identified as being too tight, and were then both set to 1×10^{-3} . This value may seem large, but when dealing with the tensor mechanics module still provides adequate constraint for the purposes of this problem.

The first case that was considered is that of the steady state, constant k_{th} , uniform LHR model. The system was initialized at a temperature of 500 K, and was then allowed to converge to a steady-state solution without convergence warnings. The von mises stress calculated through this process, which describes the impacts of all stresses that a given material experiences from the Cauchy stress tensor. The radial von mises profile at three axial locations is provided in Figure 1a and shows the peak stress directly on the rim of the fuel region. This is the expected response, as when undergoing thermal expansion while constrained by the exterior materials, this region of the fuel pellet will

experience stress while exerting pressure against these constraints. The local maximum at the center of the pellet is likely due to nature of the 2D-RZ solution where the centerline is effectively pinned from any left-hand displacement.

The thermal expansion of the system was then verified by inspection of the upper boundary on the fuel-gap-clad interface as seen in Figure 1b. At the beginning of the simulation with initial conditions, all three regions are at an identical height and temperature. Once the solution converges, a noticeable but small-in-magnitude relative difference is seen between the fuel and clad regions. This is also unsurprising, as the thermal expansion coefficient is larger for the fuel, and since the fuel is radially constrained by the smaller thermal expansion of the clad. Due to these combined effects, the fuel stack has a vertical displacement beyond the non-constraining top boundary.

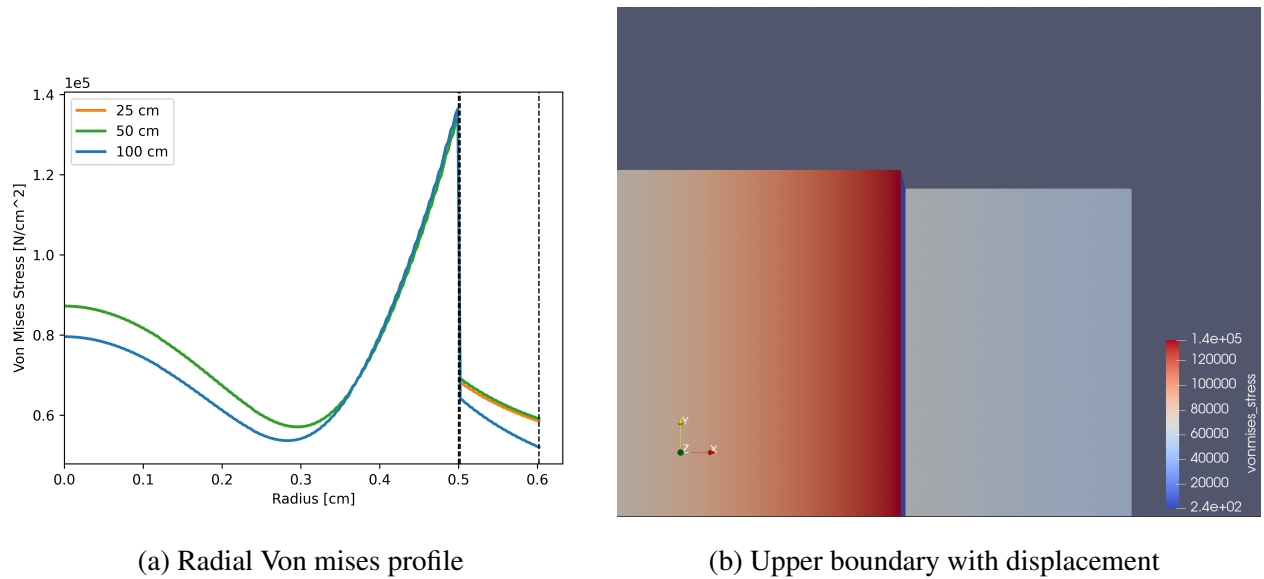
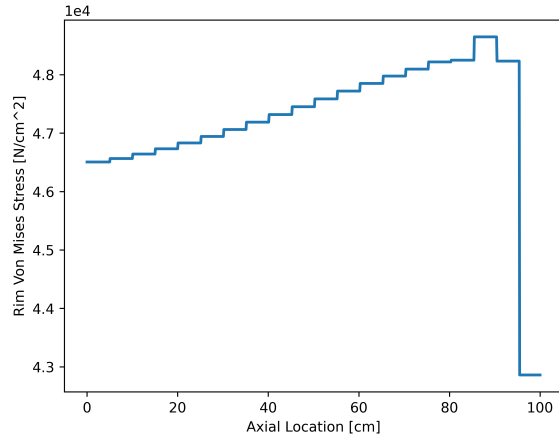
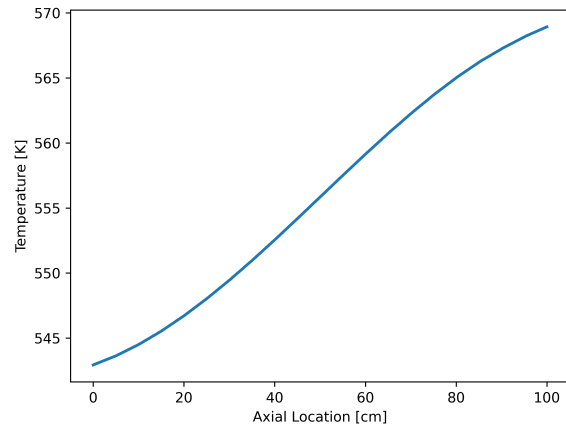


Figure 1: Steady state with constant k_{th} , uniform LHR

With the uniform LHR, the heat transfer rate is governed by the axial relationship in coolant heat transfer which becomes smaller with increasing height as the coolant heats along the rod. The von mises axial profile along the rim was then plotted for this case in Figure 2a which shows a monotonically-increasing trend with axial height until about 90 centimeters. After this point, it decays rapidly which could be caused by the proximity to the exposed region post-expansion or due to some computational artifact. Figure 2b shows the trend in rim temperature over the axial height, which agrees in trend with that of the von mises with the exception of the extreme upper location.



(a) Von mises axial profile



(b) Rim temperature axial profile

Figure 2: Steady state with constant k_{th} , uniform LHR

The steady state, constant k_{th} with varying LHR case was then considered. The radial temperature profiles and axial centerline temperature profiles were first plotted and inspected for general trend agreement in Figure 3. Both present expected values and trends when compared with those in Part II of the project. The von mises axial profile at the rim was then plotted in Figure 4a showing a parabolic trend similar to the axial temperature shape. Since the von mises stress depends directly on thermal expansion and therefore temperature, this curve appears to be correct in trend. Figure 4b shows the temperatures at the same locations of the recorded von mises values (at the rim, $x = 0.602\text{cm}$), which are cooler than the centerlines due to proximity to the cladding/working fluid.

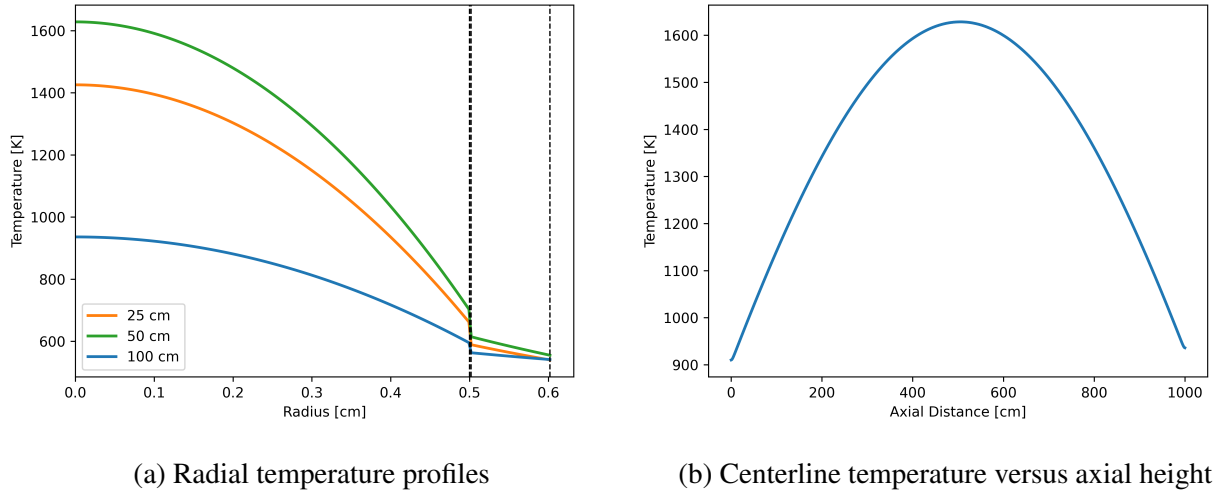


Figure 3: Steady state varying-LHR temperature curves

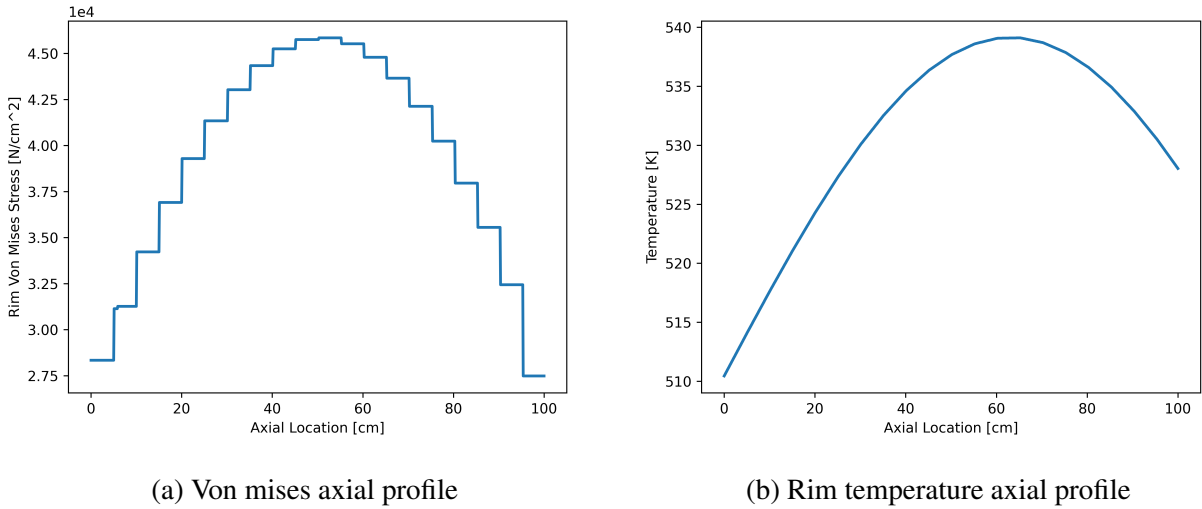


Figure 4: Steady state with constant k_{th} , varying LHR

The two cases considering temperature-dependent thermal conductivity were then run. In general, with rising temperature, the thermal conductivity of uranium dioxide decreases; the opposite however is seen with zirconium alloy species which see increasing k_{th} values with temperature. With these competing effects, a numerical solution is required to observe the overall response in the system. In the uniform LHR case, the midplane temperature profiles were plotted in Figure 5. The temperature dependent radial profile is observed to have a lower temperature in all regions when

compared to the constant-conductivity model. When assessing the thermal conductivity values for these temperatures, the temperature-dependent value of $0.191 \frac{\text{W}}{\text{cmK}}$ is greater than that of the constant 0.17 set leading to an overall more effective heat transport through the clad. In the fuel, the center region sees a smaller thermal conductivity in the temperature dependent case when compared with the constant 0.03 value. Around 1200 K, this changes with the temperature-dependent conductivity steadily increasing with temperature, which likely accounts for the lower temperatures seen throughout the region.

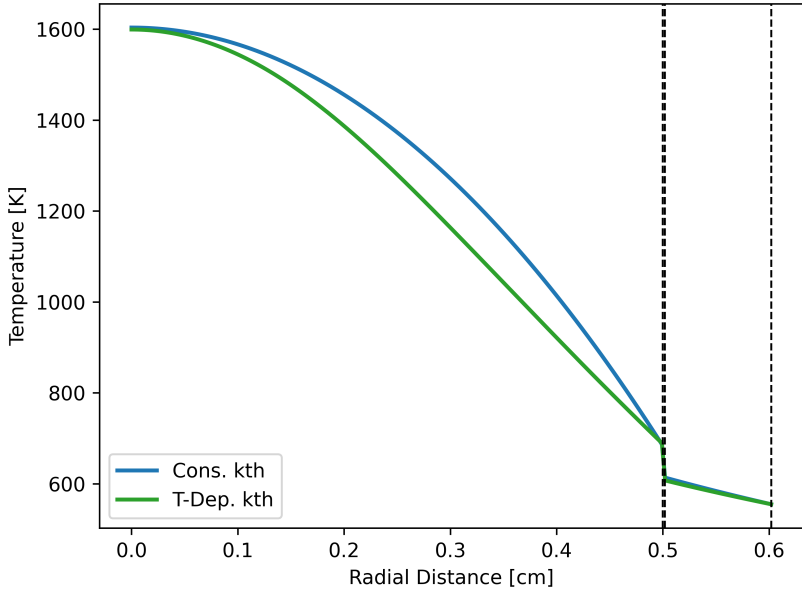


Figure 5: Comparison of constant vs. T-dependent k_{th} midplane temperature profiles

A transient case with axially-variant LHR was then considered using the LHR_0 equation provided with a time dependency. The code was altered manually to include the time derivative in the heat conduction equation, requiring the setting of material densities. With the equation, the LHR_0 value saw an initial spike to $2.50 \times 10^2 \text{ W cm}^{-1}$ from a value of 126.8, which then decayed down to $1.50 \times 10^2 \text{ W cm}^{-1}$. This led to the response seen in centerline temperatures as displayed in Figure 6a, which is plotted over [0,100] time for the elapsed transient. The maximum all-time centerline temperature was recorded as 1271.1K at a time of $t = 22$. At $t = 100$, the centerline temperature reached a maximum of 984.2K at a location of 0.9 cm above the midplane. The full curve at this time is presented in Figure 6b, illustrating the same parabolic trend but with a recovered maximum

temperature.

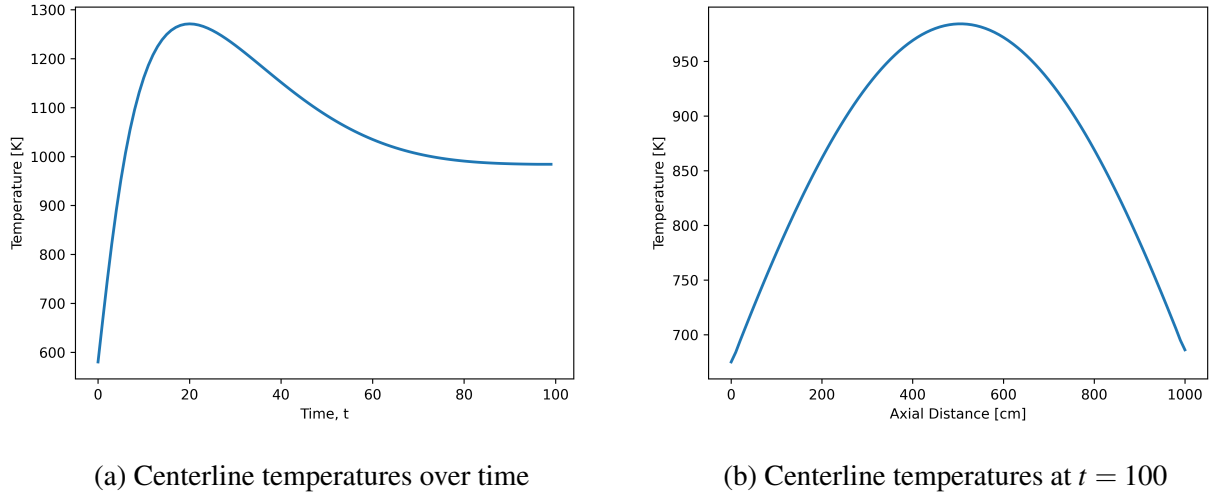
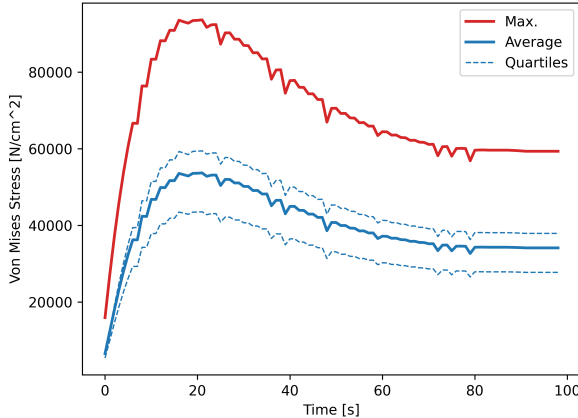
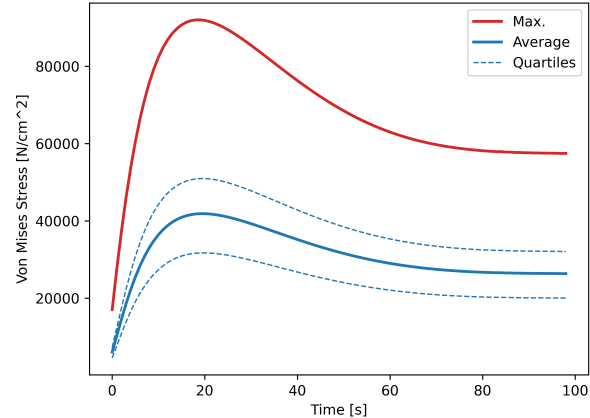


Figure 6: Transient temperature curves

This model was then run using the uniform LHR of $3.50 \times 10^2 \frac{\text{W}}{\text{cmK}}$. The von mises stresses were then collected from both models for analysis, which are shown in Figure 7 with relevant statistics. The maximum von mises stresses are nearly twice that of the average for both models with good agreement in each curve's trend (which also agrees with the temperature perturbation). There is a larger degree of noise in the uniform LHR case, which is likely due to computational causes rather than any physical interpretation. In the uniform LHR case, the von mises stresses reach a maximum at a timestep of around 20 seconds and exhibit as the double-peaked profile in Figure 8a. Again, the inner region's heightened stress is likely due to the 2D-RZ constraints in the model definitions. The highest point of stress is seen in the rim of the fuel region as expected. The profile at $t = 100$ is then shown in 8b, with a largely-recovered von mises arrangement compared to the peak.

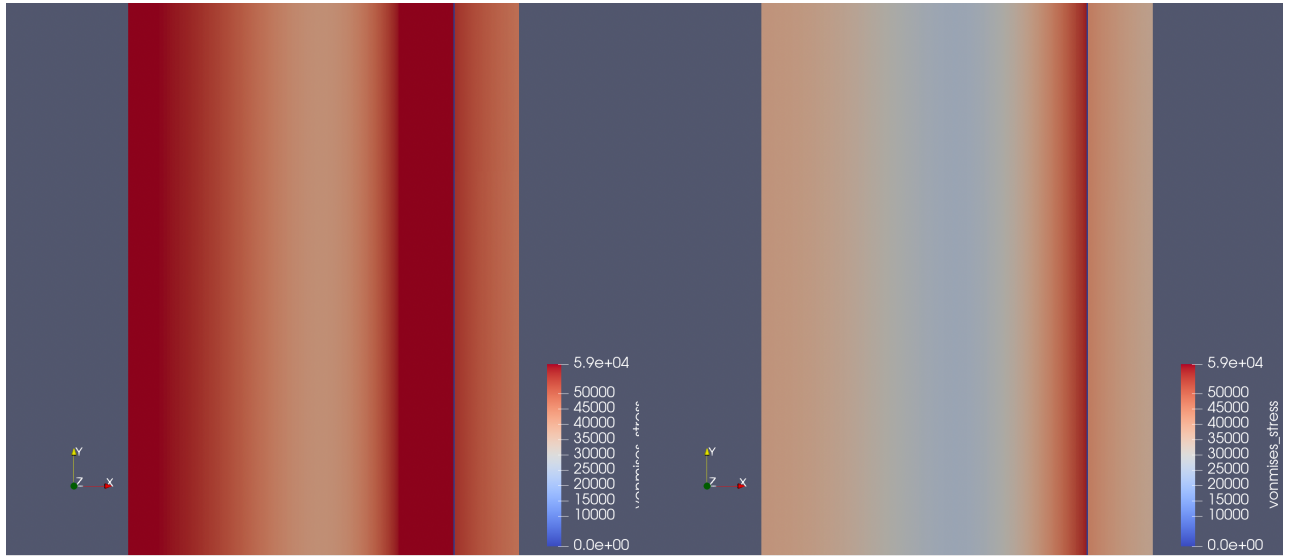


(a) Uniform LHR



(b) Axially-varying LHR

Figure 7: Transient von mises exposure



(a) Peak

(b) Recovery

Figure 8: Midplane von mises behavior during uniform LHR transient

In a final point of comparison, the uniform LHR and axially-variant LHR cases were then compared in Figure 9 with their maximum von mises stresses over the transient. During the initial peaking, both of the curves tightly agree with each other. There is a small difference in recovery responses between the two, with a slightly reduced stress in the axially-variant LHR case. Overall, there is not likely a large enough difference between these models to declare significance.

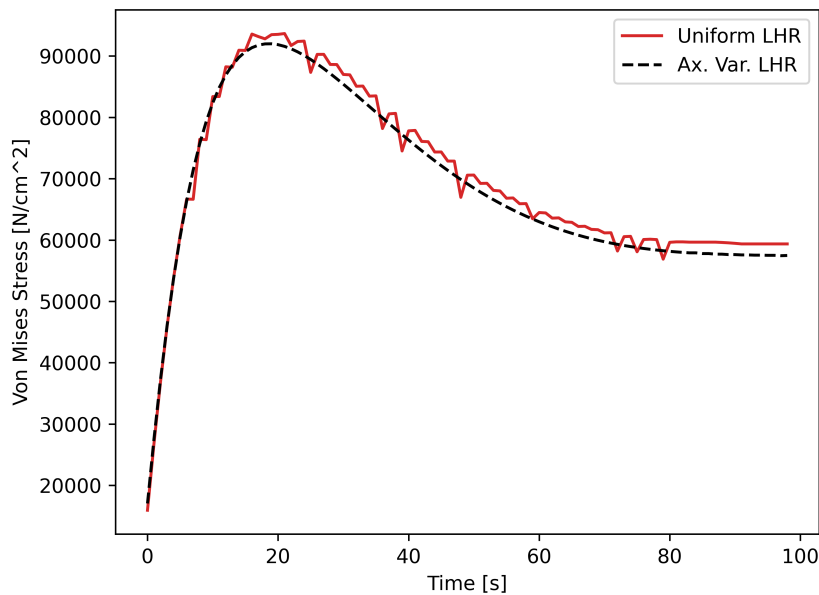


Figure 9: Comparison of uniform LHR vs. axially-variant LHR in transient

References

- [1] T. NISHIJIMA, T. KAWADA, and A. ISHIHATA, “Thermal Conductivity of Sintered UO₂ and Al₂O₃ at High Temperatures,” *Journal of the American Ceramic Society*, **48**, 1, 31–34 (1965).
- [2] J. CLEVELAND, “Thermophysical Properties of Materials for Water Cooled Reactors. IAEA-TECDOC-949,” (1997).